Weather Radar Ground Clutter. Part I: Identification, Modeling, and Simulation

J. C. HUBBERT, M. DIXON, S. M. ELLIS, AND G. MEYMARIS

National Center for Atmospheric Research, Boulder, Colorado*

(Manuscript received 29 April 2008, in final form 11 January 2009)

ABSTRACT

Real-time ground-clutter identification and subsequent filtering of clutter-contaminated data is addressed in this two-part paper. Part I focuses on the identification, modeling, and simulation of S-band ground-clutter echo. A new clutter identification parameter, clutter phase alignment (CPA), is presented. CPA is a measure primarily of the phase variability of the in-phase and quadrature-phase time series samples for a given radar resolution volume. CPA is also a function of amplitude variability of the time series. It is shown that CPA is an excellent discriminator of ground clutter versus precipitation echoes. A typically used weather model, time series simulator is shown to inadequately describe experimentally observed CPA. Thus, a new technique for the simulation of ground-clutter echo is developed that better predicts the experimentally observed CPA. Experimental data from the Denver Next Generation Weather Radar (NEXRAD) at the Denver, Colorado, Front Range Airport (KFTG), and NCAR's S-band dual-polarization Doppler radar (S-Pol) are used to illustrate CPA. In Part II, CPA is used in a fuzzy logic algorithm for improved clutter identification.

1. Introduction

Ground-clutter characteristics have been studied extensively and excellent summaries and discussion of clutter and clutter statistics are given by Long (2001) and Billingsley (2002). Ground-clutter signal and statistics vary widely since ground-clutter targets are very diverse: plants, trees, bare ground, rocks, buildings, other man-made structures, and ground snow. One way that has been used to classify and characterize ground clutter is via the amplitude statistics of clutter that are typically reported as fitting Rayleigh, Weibull, Ricean, or lognormal distributions (Long 2001). The Weibull and Ricean distributions include Rayleigh as a subclass. Ground-clutter echo fluctuations can be characterized either temporally or spatially. Temporal statistics result from data gathered at a fixed azimuth, elevation, and range (i.e., from a single resolution volume). Such amplitude statistics are usually reported as Ricean, which includes Rayleigh in one limit and more peaked distributions in the other limit (Long 2001). Ricean distributions result from the vector sum of one constant dominant scatterer surrounded by other Rayleigh fluctuating echoes (Norton et al. 1955). Limit here refers to the two extremes of the Ricean distribution parameter "m," which controls the ratio of the constant power to the average power of the surrounding fluctuating (Rayleigh) component. Spatial amplitude statistics, however, have typically been reported as being Weibull distributed (Booth 1969; Sekine and Mao 1990; Billingsley and Larrabee 1991; Long 2001), which has broader echo amplitude distributions than prescribed by Rayleigh. For radar amplitude clutter statistics that result from both temporal and spatial effects, compound distribution models have been used. Two such distributions are a Rayleigh distribution modulated by a Weibull distribution (Simkins 1984) and the K distribution (Jakeman and Pusey 1976; Jao 1984). For typical S-band weather radar scanning strategies examined here, temporal amplitude statistics are more narrowly distributed, while spatial statistics are typically more broadly distributed. However, for the practical identification of clutter, the spatial variability of the integrated mean power (i.e., reflectivity) is much more relevant than the form of the amplitude distribution. Two of the parameters used in the fuzzy logic clutter identification algorithm discussed in Hubbert et al. (2009, hereafter Part II) are measures of the clutter echo power spatial variability.

* The National Center for Atmospheric Research is sponsored by the National Science Foundation.

Corresponding author address: J. C. Hubbert, P.O. Box 3000, NCAR/EOL, Boulder, CO 80307.
E-mail: hubbert@ucar.edu

DOI: 10.1175/2009JTECHA1159.1

Here in Part I, a new parameter for identifying clutter, called the clutter phase alignment (CPA), is introduced and studied. In contrast to previous clutter identification parameters that were a measure of the variability of just the amplitude of the return time series for a radar resolution volume (Schaffner 1975; Geotis and Silver 1976), CPA is a function of not only the amplitudes of the time series but also, more importantly, the phase. In short, CPA is a measure of temporal phase fluctuations of echoes over typical data collection times for a single radar resolution volume. Thus, closely related to CPA is the velocity and spectrum width of the signal (see Bringi and Chandrasekar 2001, for definitions of mean velocity and spectrum width of weather signals). S-band signals with absolute mean velocity greater than about 3 m s^{-1} velocity have very low CPA values. In general, as the spectrum width of the signal increases, the CPA values decrease because signals with wide spectrum widths fluctuate more over the measurement period as compared to narrow spectrum width signals. Additionally, the spectrum width of ground-clutter echoes is usually quite narrow ($<$0.3 m s^{-1}), while spectrum widths of weather echoes are typically much wider ($>$1.0 m s^{-1}; Doviak and Zrnić 1993; Fang et al. 2004). Spectrum width, however, has not been a particularly effective identifier of clutter and simulations are given here that demonstrate this.

Also in this paper a new technique for simulating ground-clutter echo is given. The motivation for modeling ground clutter is twofold: 1) to simulate time series that result from ground clutter, specifically for typical weather radar data collection strategies; and 2) to gain a better understanding of experimentally observed CPA values. For weather radar, we are interested in temporal statistics that are slightly modulated by spatial statistics because of a 1° antenna beamwidth (approximately) radar scanning nominally over about 1° in azimuth. It is shown that clutter echo time series simulated using a weather model do not yield statistics that match the experimentally observed clutter statistics. Thus, a new technique for modeling and simulating ground-clutter echo is given that can better match the experimental data.

This paper is organized as follows: Section 2 discusses the problem of identifying clutter based on signal characteristics from one resolution volume. Spectrum width estimation is discussed and CPA is introduced and developed theoretically. Experimental data from the Denver Next Generation Weather Radar (NEXRAD) at the Denver, Colorado, Front Range Airport (KFTG) are used to illustrate the theory. In section 3, a new model to simulate ground-clutter time series is given, and in section 4 the signal statistics of the simulations are compared to KFTG experimental data. Section 5 summarizes and concludes this paper.

2. Ground-clutter identification

Ground-clutter echoes from stationary targets have zero-mean velocity and narrow spectrum widths and thus these attributes can be used to identify clutter. For an overview of clutter identification and mitigation in the literature, see Part II. Some clutter targets can move (e.g., wind-blown trees) and, furthermore, the radar is typically scanning rotationally, so that the actual measured velocity can vary somewhat from zero and the spectrum widths can be widened. Still, considering both wind and an antenna rotation of 10°–18° s^{-1}, Doviak and Zrnić (1993) estimate that typical spectrum widths of ground clutter are about 0.26 m s^{-1}. Since typical spectrum widths of weather echoes are greater than 1 m s^{-1} (Fang et al. 2004), spectrum width should be a good indicator of clutter.

However, the accurate estimation of such narrow spectrum widths is problematic. For typical weather radar scanning parameters at S band, the spectrum width measurement error can be very high, especially at narrow spectrum widths (Bringi and Chandrasekar 2001; Doviak and Zrnić 1993). For example, consider the histogram of spectrum width estimates shown in Fig. 1. Radar data are simulated at S band with a spectrum width of 0.5 m s^{-1}, mean velocity of 0 m s^{-1}, pulse repetition time (PRT) of 0.001 s, and a length of 64 samples (Chandrasekar et al. 1986); 50 000 time series are generated. To calculate spectrum width, the unbiased autocorrelation estimate is used (Doviak and Zrnić 1993):

$$R(i) = \frac{1}{N-i}\sum_{k=1}^{N-i} x(k)x^*(k+i), \tag{1}$$

where i is the autocorrelation lag (e.g., $i = 0$ yields power), $x(k)$ is a radar time series, N is the length of the time series, and "*" denotes complex conjugation. The so-called $R(0)/R(1)$ spectrum width estimator is

$$\sigma_v = \frac{\lambda}{2\pi T_s\sqrt{2}}\left[\ln\left|\frac{R(0)}{R(1)}\right|\right]^{1/2}, \tag{2}$$

where λ is the wavelength and T_s is the sampling period. As can be seen, when $|R(1)| > |R(0)|$ the logarithm becomes negative and the square root becomes a complex number; that is, a nonphysical width estimate is obtained. One strategy is to set the spectrum width to zero under such circumstances. Of the 50 000 simulations

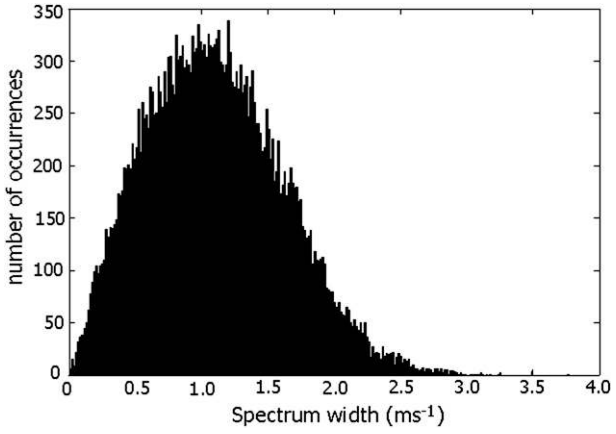

FIG. 1. Histogram of spectrum width estimates for the unbiased estimator. The simulated width is $\sigma_v = 0.5$ m s^{-1}. The number of simulations is 50 000. Of these, 28 843 had $|R(1)|$ larger than $|R(0)|$, which is a nonphysical spectrum width estimate (i.e., a square root of a negative number). If these estimates are set to zero m s^{-1}, which is sometimes done, then a bimodal distribution results.

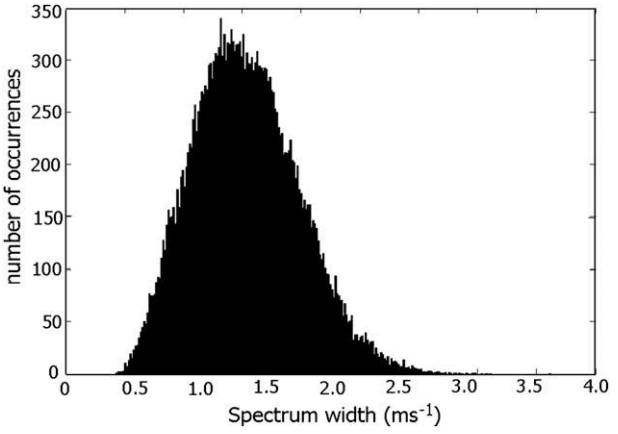

FIG. 2. Histogram of spectrum width estimates for the biased estimator for the same simulation parameters as used in Fig. 1. Here $|R(0)|$ is always larger than $|R(1)|$.

performed, 21 157 (about 42%) have $|R(1)| > |R(0)|$. The mean and standard deviation of the other 28 843 width estimates are 1.1 m s^{-1} and 0.5 m s^{-1}, respectively. Hence, the distribution of estimated spectrum widths is bimodal. These results demonstrate that spectrum width is estimated rather poorly with this estimator, and this is the reason why, in general, spectrum width estimator is not a particularly robust indicator of clutter. The fact that $|R(1)| > |R(0)|$ occurs at all can be attributed to the unbiased autocorrelation estimate used: $R(0)$ is normalized by the number of samples, that is, 64 here, whereas $R(1)$ is normalized by the number of products that contribute to the sum in Eq. (1), that is, 63 in the present case. The biased autocorrelation estimator (Bringi and Chandrasekar 2001), which normalizes both $R(0)$ and $R(1)$ by the length of the time series, that is, 64 here, could instead be used.

Using the biased autocorrelation estimate and the same simulation parameters as used for Fig. 1, the histogram shown in Fig. 2 is obtained. For these width estimates, $|R(0)|$ is always greater than $|R(1)|$, which is intuitively satisfying. However, the mean is 1.53 m s^{-1}, which is a 1.03 m s^{-1} bias, and the standard deviation is 0.45 m s^{-1}. It is also interesting that there are no spectrum width estimates below about 0.4 m s^{-1} and only a few estimates at or below the simulated spectrum width of 0.5 m s^{-1}.

Summarizing, even though ground-clutter echoes have narrow spectrum widths, the practical estimation of the widths is problematic with the commonly used estimators. The spectrum width estimates could be improved by employing other estimators that utilize more lags of the autocorrelation function (Passarelli and Siggia 1983; Meymaris and Williams 2007). The problem is that these estimators have poor performance for signals with wide spectrum widths. The higher autocorrelation lag products will be ''noisy'' because of the shortened decorrelation time due to the wide spectrum width. An additional concern is that operational radars such as the Weather Surveillance Radar-1988 Doppler (WSR-88D) typically use fewer than 64 samples to estimate mean velocity and spectrum width. Fewer times series samples typically means that the resulting estimates will have higher standard deviations which will exacerbate the above-described problem of $|R(1)| > |R(0)|$. The reader is reminded, however, that it is the number of equivalent *independent* samples and not just the total number of samples used that is critical for reduced variance of the autocorrelation estimates (Doviak and Zrnić 1993).

Simulations for spectrums widths of 0.26 m s^{-1} were also performed and the results also show that more than 40% of the simulated time series have $|R(1)| > |R(0)|$. We next present another clutter identification parameter, clutter phase alignment, that is more robust than spectrum width and also is a function of mean velocity.

a. Clutter phase alignment

The backscatter amplitudes from fixed, nonmoving targets (i.e., many ground-clutter objects) are constant. Thus, if the radar is stationary, the received base-band complex signal [referred to as the in-phase and quadrature-phase (I and Q) components] is constant. This is predicated on a coherent transmitter [e.g., a Klystron or traveling wave tube (TWT)] or on a magnetron transmitter where the transmit phase is measured for each

pulse and subsequently the received signal is corrected with this phase. Under these circumstances, the phase of the received signal θ is constant and this phase is measured by the radar as

$$\theta = \arg\{x_i\}, \tag{3}$$

where $x_i = I_i + jQ_i$ is the radar received time series with $j = \sqrt{-1}$.

This characteristic can be used to identify clutter-contaminated radar data. For moving targets, such as weather, the phase of the individual members of the time series will vary according to the mean velocity and spectrum width of the received signal. This then suggests that the sum

$$S = \left| \sum_{i=1}^{N} x_i \right| \tag{4}$$

should be high for clutter targets while being low for weather targets, other moving targets (e.g., flying birds), noise, etc., and thus, Eq. (4) should be a good discriminator of ground-clutter targets versus weather targets and other echoes including biological scatterers, noise, etc.

To account for power variation, CPA is defined as the magnitude of the vector sum of the individual time series members, x_i, divided by the sum of the magnitudes of the x_i:

$$\mathrm{CPA} = \left| \sum_{i=1}^{N} x_i \right| \Bigg/ \left[\sum_{i=1}^{N} |x_i| \right]. \tag{5}$$

Thus, CPA ranges from 0 to 1, with 1 indicating a very high probability of clutter. Intuitively, CPA is a good indicator of clutter since by definition it is a metric of the primary characteristic of a stationary ground-clutter target, that is, low variability of backscatter phase. Note that, if the phase of the x_i is constant, CPA will be 1 regardless of the behavior of the magnitude of the x_i. If the target is not completely stationary over the measurement period, the mean velocity may differ from 0 m s^{-1} and/or the width of the spectrum of the radar return signal may increase, both of which will decrease CPA to below 1. For the very large majority of radar clutter returns examined here, CPA is greater than 0.90, whereas CPA is less than 0.5 for most nonzero-velocity weather echoes. CPA is close to zero for noise. This includes both KFTG and S-band dual-polarization Doppler radar (S-Pol) data gathered over a 1° azimuth resolution (or 1° subtended central angle) with antenna rotation rates less than about 18° s^{-1}. Weather echoes with velocity magnitude <0.5 m s^{-1} (approximately) and spectrum widths less than about 0.5 m s^{-1} (e.g., stratiform rain in the zero-velocity isodop) can have CPA values in the 0.9 range (for S band and a PRT $\approx$ 0.001 s) and thus be misidentified as clutter. As a consequence of this, clutter identification parameters based on the spatial variability of clutter echo such as the reflectivity texture, the SPINchange of reflectivity variable as defined by Steiner and Smith (2002), differential reflectivity, or copolar differential phase are needed to distinguish this type of weather echo from clutter (see Part II for more information). To recapitulate, CPA is nearly always significantly less than 0.90 for weather time series that are collected over time periods that are significantly longer than the decorrelation time of the precipitation particles in the radar resolution volume.

The next set of plots illustrates the relationship between mean velocity and spectrum width and CPA via weather model simulations (Chandrasekar et al. 1986). Briefly, this weather time series simulator is a spectral domain technique that is based on the assumed statistical properties of weather echo (e.g., the spectrum is Gaussian shaped) and weather signal correlation properties. The mean velocity and spectrum width are specified input parameters and spectra are generated. Time series are obtained by using an inverse discrete Fourier transform (DFT). The following results have also been cross-checked with the simulation technique described by Frehlich and Yadlowsky (1994).

Time series simulations are made for velocities from -0.5 m s^{-1} to 0.5 m s^{-1} at 0.083 m s^{-1} steps, 100 simulations per step. The simulation parameters are: PRT = 0.001 s, $\sigma_v = 0.03$ m s^{-1}, 64 points, and signal-to-noise ratio (SNR = 60 dB). The spectrum width is made very narrow (0.03 m s^{-1}) to minimize the effect spectrum width has on the CPA estimates so that the effects of velocity are more clear. For each simulated time series the velocity is estimated (via the phase of the first lag of the autocorrelation function). The resulting scatterplot of CPA versus estimated velocity is shown in Fig. 3 (note that the simulated velocity and the estimated velocity are, in general, not the same). As can be seen, as velocity magnitude increases, the value of CPA decreases rather quickly. When the velocity magnitude is greater than 0.2 m s^{-1}, the average CPA values are below 0.9.

To see the effect of broadening the spectrum width on CPA, a scatterplot of CPA versus estimated mean velocity when the spectrum width is 0.26 m s^{-1} (an expected typical spectrum width for clutter Doviak and Zrnić 1993) is shown in Fig. 4. The simulated velocity is always zero to isolate the effects of spectrum width broadening on CPA. Otherwise, the simulated parameters are as in Fig. 3. As can be seen, there is

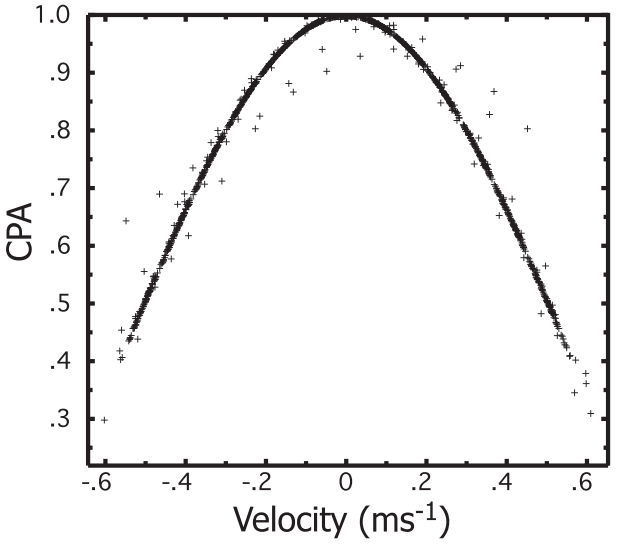

FIG. 3. Scatterplot of CPA vs estimated velocity for simulated data. The simulated width is $\sigma_v = 0.03$ m s^{-1} and the mean velocity ranges from -0.5 to $+0.5$ m s^{-1}, with 0.083 m s^{-1} increments. The number of simulations is 1300, with 100 simulations per velocity increment.

considerable scatter with a significant number of points having CPA values less than 0.90 and the estimated velocities range from -0.4 m s^{-1} to $+0.4$ m s^{-1}. Shown in Fig. 5 is a cumulative histogram of the data shown in Fig. 4 which is normalized by the total number of points.

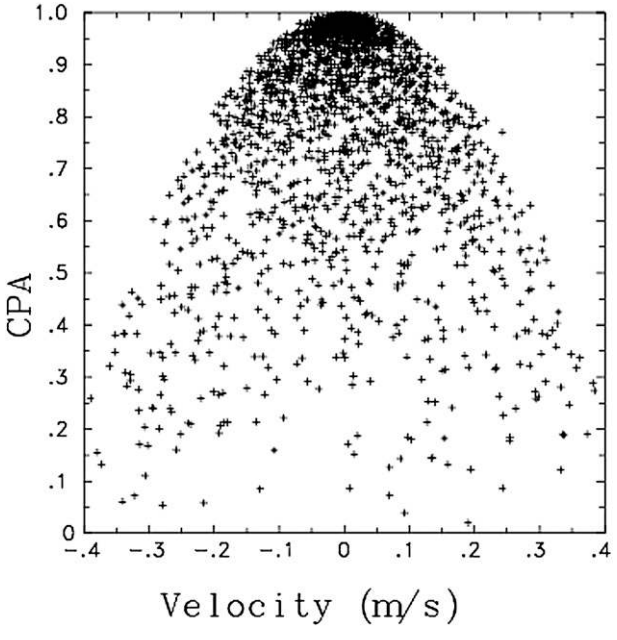

FIG. 4. Scatterplot of CPA vs estimated velocity for simulated data. The simulated width is $\sigma_v = 0.26$ m s^{-1} and the velocity is $v = 0.0$ m s^{-1}. The number of simulations is 2500.

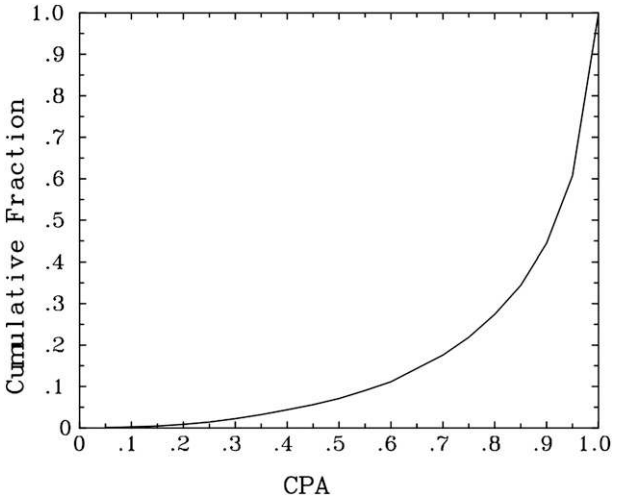

FIG. 5. Cumulative histogram of data shown in Fig. 4. The number of occurrence is normalized by the total number of occurrences so that a cumulative fraction results.

More than 25% of the points have CPA values of less than 0.8. Experimental ground-clutter data using S-Pol or KFTG do not agree with this plot, which is shown below.

Figure 6 illustrates the relationship between CPA and mean velocity and spectrum width for widths more typical of weather. Shown are six scatterplots of CPA versus mean velocity for spectrum widths of 1, 2, 3, 4, 5, and 6 m s^{-1} in Figs. 6a–f, respectively. There are 5100 data points per graph and the simulated velocities are distributed equally between plus and minus the Nyquist velocity of 26.7 m s^{-1}. As the spectrum width increases, the distribution of elevated CPA values becomes broader and the average CPA for the points with velocity close to 0 m s^{-1} decreases. Importantly for discrimination between clutter and precipitation echo, the large majority of CPA values are below 0.6 for all plots.

Figure 7 shows a KFTG 0.5° plan position indicator (PPI) clear-air surveillance scan of reflectivity [the NEXRAD scan strategy volume control pattern (VCP) 32]. The data were gathered at 2123 UTC 13 October 2006. The large reflectivities on the left are caused by the Rocky Mountains. The antenna was scanning at 6.5° s^{-1} with about 64 time series samples per degree azimuth. Shown in Fig. 8 is a two-dimensional color histogram scatterplot of the experimentally measured CPA values. There are about 19 000 data points and, as can be seen in the color histogram, the majority of the points are confined to the region -0.1 m s^{-1} $<$ velocity $<$ 0.1 m s^{-1} and CPA > 0.95. The data of Fig. 8 are more concentrated at CPA values >0.9 and the spread in the velocities is lower than for the data shown in Fig. 4. Figure 9 shows three normalized, cumulative

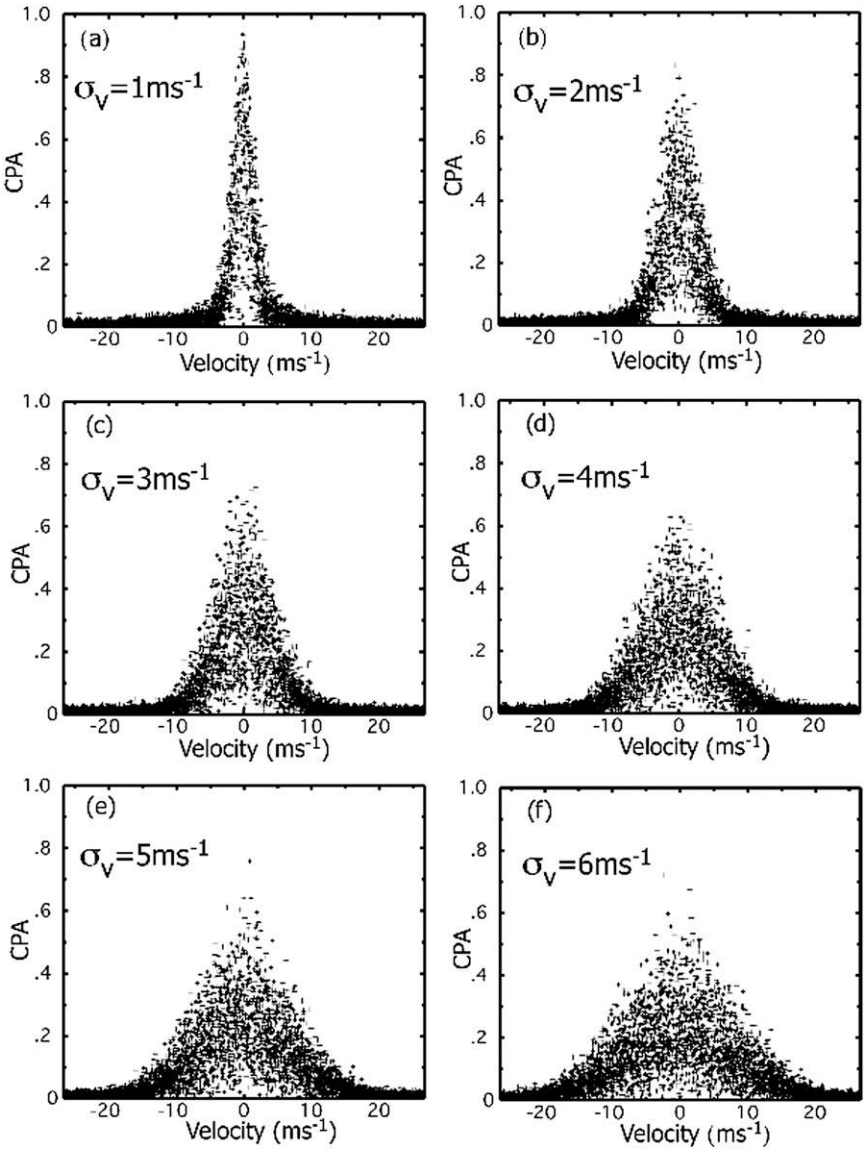

FIG. 6. CPA vs estimated velocity scatterplots for simulated data. The spectrum widths (σ_v) vary from 1 to 6 m s^{-1} as shown. There are 5100 data points per graph and the requested velocities are evenly distributed between plus and minus the Nyquist velocity of 26.7 m s^{-1}.

histograms for the data in Fig. 8 (and three curves from modeled data to be discussed later). CPA is calculated from time series lengths of 64, 32, and 16, which correspond to antenna subtended scan angles of 1.0°, 0.5°, and 0.25°, respectively. As can be seen, the narrower the subtended scan angle, the higher the CPA. This set of curves illustrates the effect of the size of the scanning angle on CPA. The curve from Fig. 5 is included for ease of comparison (labeled weather model). The histogram shows that, for CPA < 0.8, the cumulative fraction of CPA values for the 64-point experimental curve and weather model curve are 0.09 and 0.28, respectively. There are two possible explanations for this discrepancy. One is that most of the clutter echo spectrum widths are much narrower than 0.26 m s^{-1}. The other is that clutter is not well modeled using the same simulation algorithm as is used for weather signals. The simulated spectrum width for the weather model can be reduced to 0.14 m s^{-1} so that the resulting CPA cumulative histogram matches quite well with the 1° experimental cumulative histogram of Fig. 9. However, it is shown later that the resulting scatterplot of CPA versus

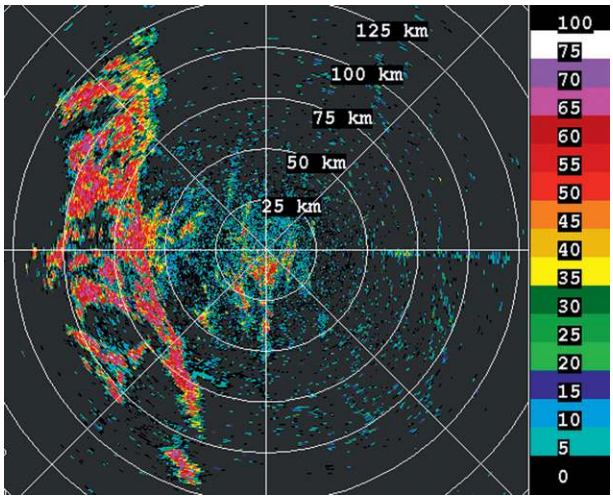

FIG. 7. A KFTG clear-air PPI surveillance reflectivity scan showing ground clutter. The data were gathered at 2123 UTC 13 Oct 2006. The large reflectivities seen on the left are from the Rocky Mountains.

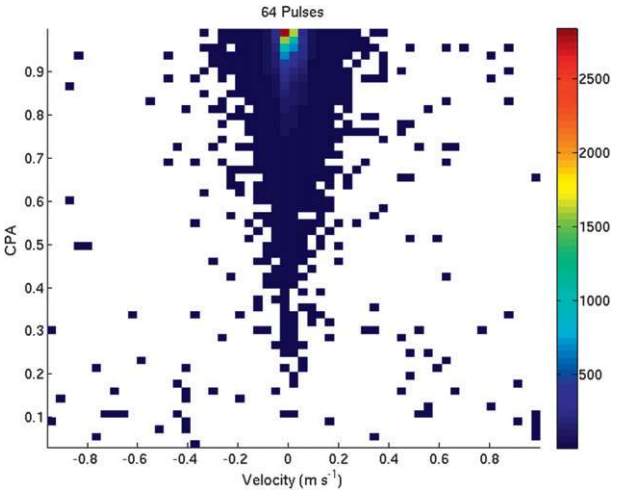

FIG. 8. A histogram scatterplot of CPA vs radial velocity for data shown in Fig. 7. The colors denote the number of occurrences. There are 18 958 points.

velocity for data from the weather model does not then agree with the similar experimental scatterplots. In section 3, a new method for modeling ground clutter is presented that better predicts the characteristics of the experimentally observed CPA. Data from the new clutter model are given in Fig. 9 for reference, but these results are discussed later after the new clutter model is presented.

In summary, both velocity and spectrum width affect CPA: 1) as the velocity departs from zero, CPA decreases rapidly; 2) as the spectrum width increases, the value of CPA, in general, decreases. There are well-known variances associated with the pulse pair velocity estimator and especially the width estimator as shown earlier in this paper. Furthermore, no particular spectrum shape is assumed for the CPA calculation as is assumed with the pulse pair estimators. An additional advantage is that CPA can be directly calculated from staggered PRT time series, which makes it viable for such data. For these reasons, CPA is a more robust and versatile indicator of clutter than a combination of radial velocity and spectrum width.

Finally, the spectrum width of clutter echoes depends upon the radar location (i.e., the characteristics of the surrounding clutter targets), the rotational scan rate, and any movement of the clutter (e.g., due to winds). Thus, the experimental data reported here are specific to the Colorado Front Range clutter environment. The clutter targets are predominantly in the foothills of the Rocky Mountains, but there are also prairie and significant deciduous tree and shrub vegetation targets, especially in the more populated regions. Nevertheless, CPA from radar data from other geographical regions should be examined. We have used clutter mitigation decision (CMD) with S-band data from the Centre for Australian Weather and Climate Research CP-2 radar (Keenan et al. 2006) and with S-Pol data from the recent National Center for Atmospheric Research (NCAR) field campaign, Terrain-influenced Monsoon Rainfall Experiment (TiMREX) in Taiwan. The clutter from both radar sites, especially the Taiwan site, is dominated by deciduous, tree-covered hills and mountains. Preliminary results indicate that CPA performed

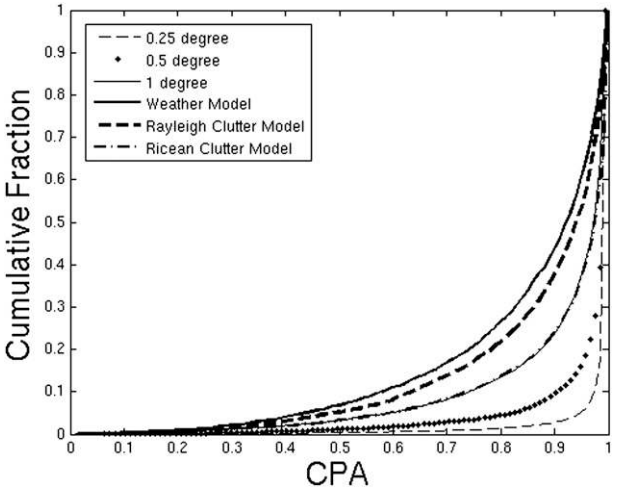

FIG. 9. Cumulative histograms of experimental CPA values from data shown in Fig. 7 for subtended scanning angles of 0.25°, 0.5°, and 1.0°. Cumulative histograms of modeled data are also overlaid. The curve due to the RiM lies nearly on top of the experimental 1° curve.

well in these environments. Also, the KFTG data of Fig. 8 was gathered at a 6.5° s^{-1} rotation rate, which indirectly affects the spectrum width of clutter echoes. However, as demonstrated in Fig. 9, it is the scanning angle subtended by the radar during the time series collection period that causes CPA to decrease (equivalently, an increase the spectrum width) rather than the radar scanning rate per se. Data shown in both Part I (this paper) and Part II are for radar resolution volumes of 1° in azimuth, unless stated otherwise. Thus, the statistics of CPA, spectrum width mean velocity estimates (*for clutter*) will be about the same for rotation rates from 6.5° s^{-1} to 18° s^{-1}. Faster scan rates for 1° azimuth resolution volumes dictates a shortened measurement time period. This will increase measurement standard deviation of velocity and spectrum width for weather signals because fewer independent samples are gathered.

b. CPA and a spectrum power ratio

There is a relationship between CPA and the spectrum of the signal. Consider the DFT of the time series x_i,

$$X_m = \sum_{i=0}^{N-1} x_i \exp^{-j2\pi mi/N}, \tag{6}$$

where j is $\sqrt{-1}$, N is the length of the time series, and m is the frequency (velocity) index. Evaluating Eq. (6) for $m = 0$ (the zero-velocity component) yields

$$X_0 = \sum_{i=0}^{N-1} x_i \exp^{-j2\pi 0i/N} = \sum_{i=0}^{N-1} x_i. \tag{7}$$

Thus, the numerator of CPA is just the magnitude of the zero-velocity component of the DFT, namely, $|X_0|$. It is natural, then, to compare CPA to the ratio of the power of the 0 velocity component of the DFT normalized by the total power of the signal. This is referred to as the power ratio (PR). Closer examination of the CPA for consistency and $PR^{0.5}$ shows that the denominator of CPA is the L-1 norm while the denominator of $PR^{0.5}$ is the L-2 norm of the time series. While this is a rather simple difference between the two clutter metrics, it does make CPA a more effective clutter identification metric. It can be shown (see the appendix) that

$$\text{CPA} \geq \sqrt{(\text{PR})}. \tag{8}$$

This result suggests that CPA should be a better discriminator of clutter than $PR^{0.5}$ since both CPA and $PR^{0.5}$ are quite low for weather signals. If CPA is larger than $PR^{0.5}$ for clutter echoes, then CPA may distinguish better between clutter and weather echoes. To illustrate this, examine Fig. 10, which shows a scatterplot of CPA versus $PR^{0.5}$ for a low-level PPI scan that contains both clutter and weather echoes collected by KFTG at 1202 UTC 26 October 2006. A rectangular window is used for the time series. Ovals mark regions where the majority of the scatter is either from clutter or precipitation. As can be seen, there exist many resolution volumes where the $PR^{0.5}$ is in the 0.5–0.8 range while CPA is close to one. Note also that, for the resolution volumes that likely contain weather (CPA < 0.6), CPA and $PR^{0.5}$ are in closer in value. Next the time series of one of these data points is examined. Figure 11 shows the times series of $I^2 + Q^2$ dB and $\tan^{-1}(Q/I)$ degrees for a resolution volume with clutter where CPA = 0.99 but $PR^{0.5} = 0.76$ (time series length 64). The power increases more than 40 dB across the plot while the phase is contained between 0° and −20° after the twentieth sample. The plot suggests that the clutter target is entering the main lobe of the radar antenna as the radar scans. The difference between CPA and $PR^{0.5}$ can be explained as follows. Since the ground-clutter target is only visible through about half of the I and Q samples, the power time series varies dramatically from −85 to −55 dBm during which the phase remains fairly constant. This sharp gradient in the power time series spreads power away from the zero-velocity component in the spectrum of the signal, thereby reducing $PR^{0.5}$. In contrast, the low variability of the phase weighted by the high power causes CPA to be high. This characteristic makes CPA a better discriminator of clutter for such scanned ground-clutter targets. Later, we use receiver operating characteristic (ROC) curves to further demonstrate this.

3. Modeling ground clutter for simulations

Even though the physics of backscatter from ground clutter is dissimilar from precipitation, it has been suggested that clutter echo from a scanning radar can be practically modeled as zero-velocity, narrow spectrum width weather (Nguyen et al. 2008; May and Strauch 1998). An alternate approach is presented here. The simulation technique is not based on a theory of electromagnetic scattering per se as is done in Ruck et al. (1970). Rather, we give a heuristic model based on observed clutter data and use a Monte Carlo technique.

As a point of reference, for echo from precipitation particles, the I and Q signal components are independent, zero-mean Gaussian random variables (Bringi and Chandrasekar 2001). Their magnitude is Rayleigh distributed while the corresponding power is exponentially distributed and is sometimes referred to as a Rayleigh

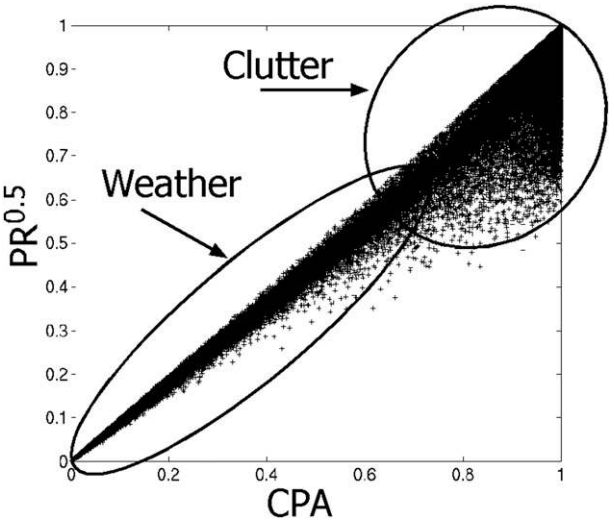

FIG. 10. Scatterplot of CPA vs $PR^{0.5}$ for the Denver NEXRAD KFTG experimental data. The data were collected by KFTG at 1202 UTC 26 Oct 2006. A rectangular time series window is used.

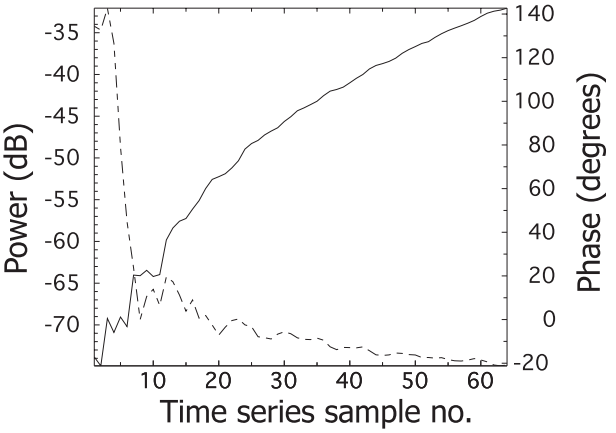

FIG. 11. Time series of power, $I^2 + Q^2$ (solid line, unitless in dB), and $\tan^{-1}(Q/I)$ (phase of I and Q, dashed line) for a resolution volume with a clutter target. CPA is 0.99 while $PR^{0.5}$ is 0.76. Time series length is 64.

power density function (Long 2001). Ground-clutter echo amplitude statistics are somewhat similar to this in that they have been observed to sometimes have a Rayleigh distribution. Physically, however, ground-clutter scattering from a myriad of diverse, nonmoving or at least zero-mean average velocity (trees may sway but do not "move") objects bears little resemblance to a collection of reshuffling precipitation particles.

a. A Rayleigh clutter model

We begin by assuming that the clutter seen by a scanning radar for a particular resolution volume can be modeled by a series of independent scattering centers that are equally spaced in azimuth angle and possess constant amplitude and phase over the measurement period (i.e., they are completely stationary). Thus, if the radar stares (i.e., is motionless during the measurement period) at a collection of such scatterers, the return measured echo would be a constant. Each scattering center is assumed to be composed of scatter from many independent scattering objects, and it is assumed that the clutter center scattering amplitudes are independent and identically distributed random variables.

Based on these assumptions and experimental observations, the clutter centers are modeled as having their magnitudes Rayleigh distributed and phases uniform random ($\pm\pi$) distributed and independent of the magnitudes. Thus, series of Rayleigh-distributed, complex scattering amplitudes a_i are generated to model clutter spatially. Next, the radar beam shape is modeled as a one-dimensional Gaussian curve with a 3-dB beamwidth of 1°. Using a Gaussian shape curve to model the main lobe of pencil-beam-type antenna patterns is common (Bogush 1989). The radar beam is truncated at ±1.5° from its center and is considered to have a constant phase pattern. The antenna beam pattern is then convolved with the scattering centers to create a time series representation of the clutter signal as seen by the radar for that resolution volume. Mathematically, the Rayleigh clutter model (RaM) is defined as

$$\alpha_k = \sum_{i=1}^{N} a_{i+k}\beta_i W_i, \tag{9}$$

where α_k is the time series, a_i are the clutter scatter centers with Rayleigh-distributed amplitudes, β_i are the antenna beam pattern weight, W_i accounts for the window used to process the time series (e.g., rectangular, Von Hann, Blackman, etc.), and N is the number of integration points (determined by the number of digitized antenna beam points). For the results presented here, a rectangular window function is used and 64 points per degree azimuth are used. Figure 12 depicts this model. There are 256 scattering centers and the antenna beam is discretized to 192 points or 3°. For each new time series point, the antenna pattern is advanced one scatter center point and the antenna pattern is multiplied with the scattering centers and summed; that is, the antenna pattern is simply convolved with the scattering centers. As is shown later, this model does not yield CPA values that match well with the experimentally observed CPA values and thus we seek to refine the RaM.

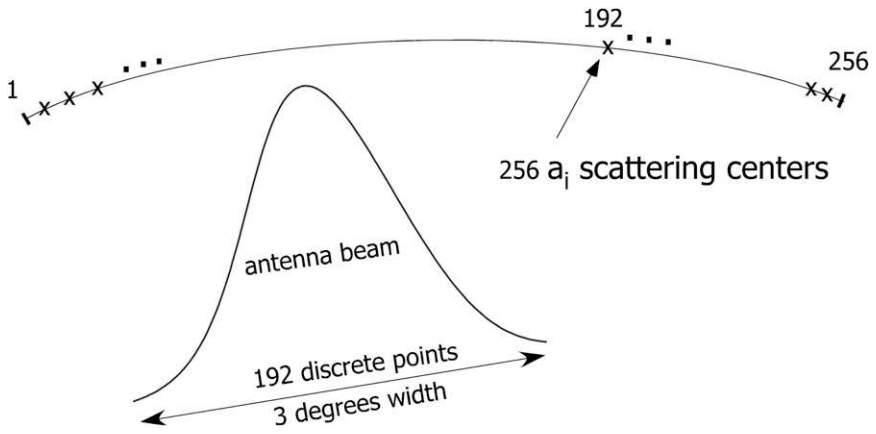

FIG. 12. An illustration of the technique used for ground-clutter time series simulations. The a_i are scattering centers. The antenna beam is modeled as a 1D Gaussian curve. The antenna beam is convolved with the scattering centers to generate the time series.

b. A Ricean clutter model

Temporal ground-clutter amplitude statistics have been reported to follow Ricean distributions (Kerr 1951; Long 2001). Ricean distributions occur when a constant vector is added to Rayleigh fluctuations. Physically, this can be interpreted as having a relatively large dominant clutter target surrounded by smaller Rayleigh-distributed scattering centers. To incorporate this effect into the RaM model, one of the scattering centers can be replaced by a larger constant, C. The magnitude of C is adjusted until the resulting CPA cumulative histogram matches the experimental cumulative histogram. The dominant scattering center is placed uniform randomly in one of the central 108 locations out of the 256 scatter center locations. The C is modeled as a Gaussian random variable (RV) with a mean of 28 and a standard deviation of 10. These are unitless numbers and are relative to the amplitudes of the Rayleigh-distributed scattering centers.[1] These values are arrived at heuristically by adjusting C until the cumulative distribution of CPA for experimental data is matched.

c. A modulated Ricean clutter model

Much ground clutter can and does move to some extent during the radar measurement period, which is approximately 64 ms in this study. This would be manifest as a small variation in the phase and magnitude of the clutter centers a_i during the measurement period. One way to model this movement is to allow the magnitude and phase of the scattering centers to vary in a random fashion as a function of k, the discrete time index. Let $a_i = m_i e^{j\phi_i}$, where m_i is the magnitude and ϕ_i is the phase of the complex scattering center a_i. The magnitude and phase of the a_i are modulated for each increment in k as

$$\hat{m}_i(k) = m_i + N(0, s_i), \tag{10}$$

$$\hat{\phi}_i(k) = \phi_i + N(0, d_i), \tag{11}$$

where $N(0, s_i)$ are independent and identically distributed (i.i.d.) Gaussian random variables with zero mean and a standard deviation that is proportional to the m_i; that is, $s_i = fm_i$ where f is the fraction of m_i for specifying one standard deviation. Here $N(0, d_i)$ are i.i.d. Gaussian random variables with zero mean and standard deviation of d degrees. The primary purpose of this model is to investigate the effect of movement of the targets in the radar resolution volume on CPA (e.g., trees swaying in the wind).

d. Simulation algorithm

The ground-clutter time series simulation scheme is as follows:

1) Create a sequence of i.i.d. Rayleigh-distributed scattering centers long enough to accommodate the number of discrete radar beam points plus the desired length of the resultant time series α_k. As used here, this is 257. Replace one scattering center with a large constant number if Ricean statistics are desired. The replacement center location is chosen as a

[1] The scattering centers are created by generating two normal i.i.d. RVs, $N_1(0, 1)$ and $N_2(0, 1)$. The RV $(N_1^2 + N_2^2)^{1/2}$ is Rayleigh distributed, while the phase RV $\arg\{N_2/N_1\}$ is uniform random between 0 and 2π.

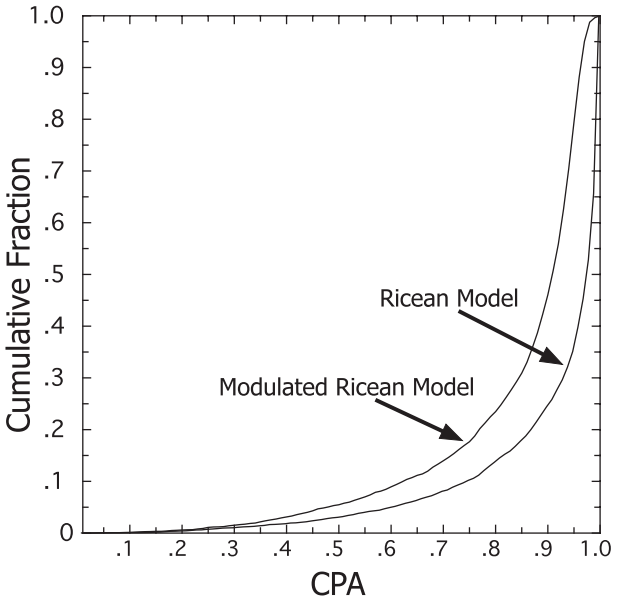

FIG. 13. Cumulative histogram of CPA for the RiM and the MRM.

uniform random variable. The magnitude of the replacement center is a Gaussian random variable, in the present case $N(28, 10)$.

2) Convolve the antenna beam with the sequence of scattering centers [i.e., $k = 1$ in Eq. (9)] to create the first time series member α_1.
3) Increment k and, if modulated statistics are desired (i.e., modeling some clutter movement), the magnitude and phase of all scattering centers are varied according to Eqs. (10) and (11).
4) Perform the convolution of the beam pattern and scattering centers to obtain the next member of the time series α_i.
5) Repeat steps 3 and 4 to create the time series α_i.
6) Compute CPA and other parameters from the constructed time series.
7) Repeat process beginning with step 1 for additional time series.

4. Using clutter models to investigate CPA

In this section results are shown for 1) the RaM, 2) the Ricean model (RiM), and 3) the modulated Ricean model (MRM) clutter simulators. Time series of length 64 are generated, the radar beamwidth is 1°, the scan angle subtended is 1°, and 5000 time series are simulated. Shown in Fig. 9 is the cumulative histogram of the CPA values for the RaM and RiM. As can be seen, the cumulative fraction of CPA from the RaM simulations is lower than the shown weather model simulation results (spectrum width is 0.26 m s^{-1}). However, the RaM cumulative fraction is still significantly higher than that of the experimental 1° data shown. The implication is that clutter observed by KFTG (and S-Pol) are not modeled well by a simple collection of Rayleigh-distributed scattering centers. The resulting CPA values are too low. Now consider the cumulative histogram from the RiM simulations in Fig. 9. As can be seen, when a large dominant scattering center is added to the Rayleigh model (thus creating the RiM model), the CPA values can be made to match the experimental CPA cumulative histogram well. This suggests that the majority of clutter seen by KFTG is typically dominated by a single ''target'' that has nearly constant backscatter phase over the measurement period.

Results from the MRM simulator are discussed next. Figure 13 shows the cumulative histogram for the MRM simulations and for modulation parameters $f = 0.20$ for the magnitude and $d = 20°$ for the phase along with the RiM simulation curve from Fig. 9 for comparison. As can be seen, the fraction of smaller CPA values does increase relative to the RiM curve. For CPA = 0.6, the cumulative fraction increases from about 0.055 for the RiM to about 0.095 to the MRM. While this is a significant increase, MRM demonstrates that the phases and magnitudes of the scattering centers can vary significantly while CPA remains high and continues to be an effective clutter identification parameter. The 20° of phase shift at S band only represents about 0.6 cm of target displacement; however, if this displacement occurs over one PRT interval of 0.001 s, it represents velocities of 6 m s^{-1}. Additionally, since the clutter center phases are modulated by a Gaussian random variable with 20° standard deviation, the phase difference of a scattering center from one time step to the next can easily be much more than 20° (the variance of the sum of two independent random variables is the sum of the variances). The experimentally measured CPA values presented here indicate that the time series phases are distributed such that the estimated mean velocity over the measurement period is close to zero (see Fig. 8). This is important to maintain high CPA values as the simulations in Figs. 3 and 4 indicate. This is examined further next.

The simulation models can be further compared by examining scatterplots of CPA versus velocity. Shown in Figs. 14–16 are such plots for experimental data, the weather model, and the RiM, respectively. The parameters used for the weather model are as before except that the spectrum width is chosen to be 0.14 m s^{-1} so that the resulting cumulative histogram of CPA values matches the 1° experimental curve of Fig. 9

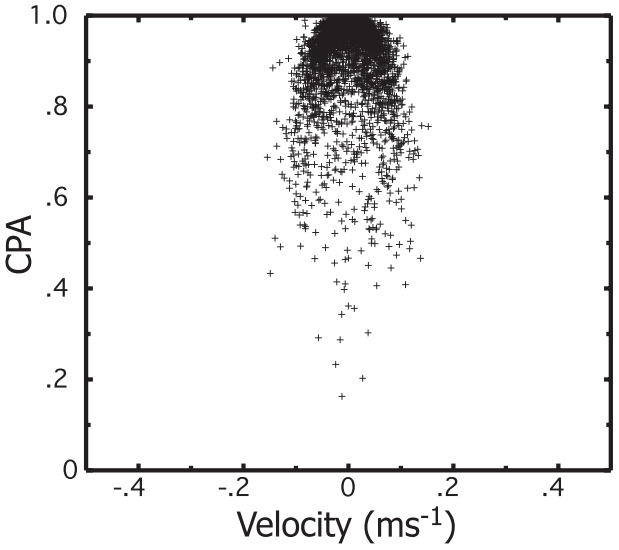

FIG. 14. Scatterplot of CPA vs velocity from experimental KFTG data. This plot uses a subset of the data from Fig. 8 but is shown again as a simple scatterplot with only 5000 points so that it can easily be compared to the simulation plots in Figs. 15 and 16.

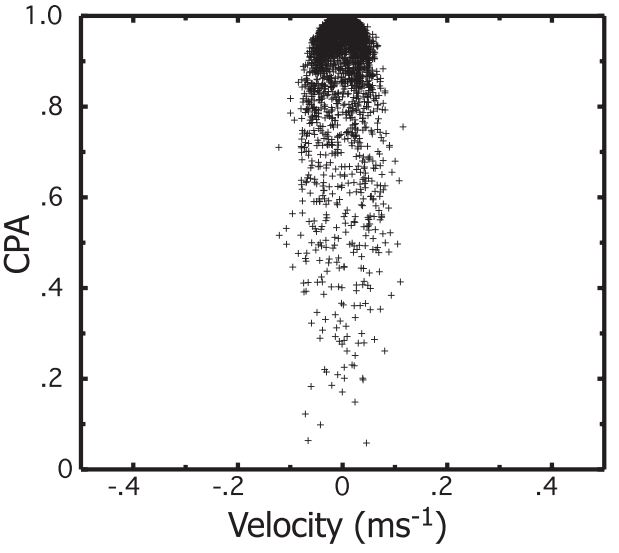

FIG. 16. Scatterplot of CPA vs radial velocity from simulated data using the clutter RiM.

well. Comparing the experimental plot of Fig. 14 to the weather model plot of Fig. 15 shows that even though the cumulative CPA histogram of the weather model data can be well matched to the experimental data, the distribution of the estimated velocities is different. This indicates that the simulated time series of clutter echo using a weather model with narrow spectrum width does not capture all of the characteristics of typical ground-clutter echo. By contrast, the CPA versus velocity scatterplot due to the RiM simulation (Fig. 16) matches the experimental velocity scatterplot (Fig. 14) better.

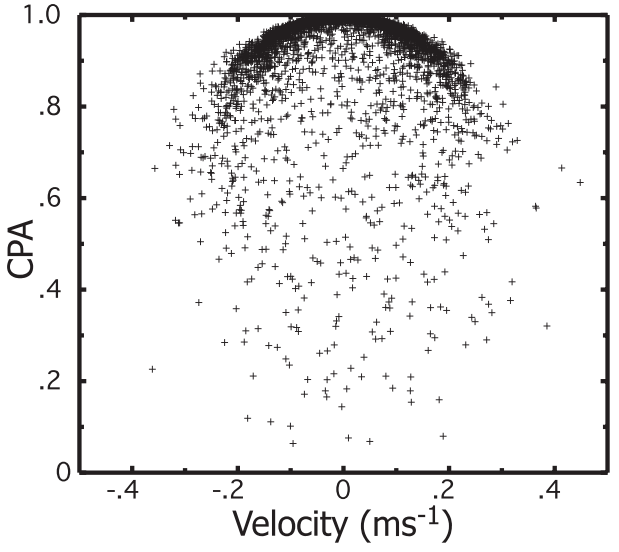

FIG. 15. Scatterplot of CPA vs radial velocity from simulated data using the weather model. The spectrum width is 0.14 m s^{-1}.

5. An evaluation of discrimination capability

The utility of a clutter identification metric is its ability to discriminate between clutter and weather echoes. One way to do this is to create histograms of clutter-only and weather-only data and then overlay the histograms. The degree of overlap of the two histograms indicates how well the metric can distinguish between the two classes of data. Here, experimental KFTG data gathered at 0954 UTC 10 October 2006 are used to create the histograms. There are about 38 600 weather data points and 13 200 clutter data points. Both stratiform and convective weather are included. Weather spectrum widths vary from very small to 6 m s^{-1} with the majority being between 0.5 and 3 m s^{-1}. Thus, the data used should be reasonably representative of weather and clutter typically observed by KFTG.

The clutter metrics evaluated are CPA, $PR^{0.5}$, and the mean value of the absolute pulse-to-pulse amplitude differences of the time series in log space (MVAR) (Geotis and Silver 1976). Thus, all three metrics are based on the sample-to-sample variability of the time series and it is of interest to compare their clutter-versus-weather discrimination capabilities. Histograms of the clutter and weather data for CPA, $PR^{0.5}$, and MVAR

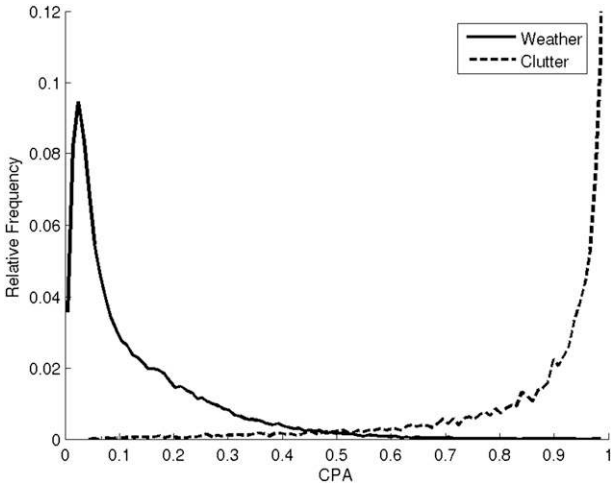

FIG. 17. Relative frequency histograms of KFTG experimental data for CPA. The data were gathered by KFTG at 0954 UTC 10 Oct 2006.

are shown in Figs. 17, 18, and 19, respectively. Comparing the degree of overlap of the clutter and weather histograms in each figure, it is fairly evident that CPA out performs MVAR and $PR^{0.5}$. To illustrate this more clearly, relative operating characteristic (ROC) curves (also known as receiver operating characteristic curves) are constructed from the given histogram plots and these are shown in Fig. 20. ROC analysis has its origin in statistical decision theory developed during World War II for the analysis of radar images (Green and Swets 1966). The ROC curves show the fraction of true identified clutter versus the fraction of weather incorrectly identified as clutter as a function of the metric. Specifically, a point on the CPA or $PR^{0.5}$ ROC curves is defined here as

$$(x, y) = [P(\alpha > \text{thres}|\text{Weather}), P(\alpha > \text{thres}|\text{Clutter})] \quad (12)$$

based on given sample populations where α is either CPA or $PR^{0.5}$, ''thres'' is a value of the metric, and P is probability. The vertical bar indicates conditional probability. The inequalities reverse for MVAR since MVAR is low for clutter and high for weather in contrast to CPA and $PR^{0.5}$. We would like to positively identify as much of the clutter population as possibly (''true positives'') while not identifying weather as clutter (''false positives''). This means that the closer a ROC curve is to the (0, 1) point on the ROC graph (upper left-hand point), the better the discrimination between clutter and weather data. At the (0, 1) point all clutter data are positively identified while no weather data are falsely identified as clutter. For reference, the dashed horizontal lines of Fig. 20 mark the location of the lower and upper break-point values for the CPA fuzzy logic membership function (see Part II of this paper for the CPA membership function). Normally both axes on a ROC curve go from 0 to 1, but we have zoomed into the area of interest for ease of comparison. Since the CPA ROC curve lies above the MVAR and $PR^{0.5}$ ROC curves, this then shows that CPA is a better discriminator of clutter and weather as compared to MVAR or $PR^{0.5}$ for the datasets used.

6. Summary and conclusions

The identification of ground-clutter echoes from the radar received time series (in-phase and quadrature-phase samples) was discussed. The spectrum width of ground-clutter echoes is typically much narrower than the spectrum width of weather echoes but spectrum width has not been a robust discriminator of weather and clutter echoes because of the large variance associated with spectrum width estimators. A new clutter identification parameter, clutter phase alignment (CPA), was introduced and examined theoretically. It was shown that CPA is affected by both spectrum width and mean velocity but is a more robust indicator of clutter than a combination of both. CPA is a good identifier of clutter echoes since it is a metric of the primary characteristic of ground-clutter echo from stationary targets: low variance of backscatter phase over typical weather radar measurement times and resolutions (1° subtended scan angle for a 1° antenna beamwidth and about 64 ms dwell time). It was observed that, for shorter subtended scan angles, the CPA values increased. This indicates that the convolution of the radar antenna pattern with the ground-clutter targets over the resolution volume is chiefly responsible for the decorrelation of the time series and the broadening of the spectrum. In contrast, the spectrum width of weather echoes is more a function of the relative velocities of the precipitation particles. Based on this observation, a Monte Carlo clutter echo simulator was introduced that models ground clutter with discrete scattering centers uniformly distributed over the scanned resolution volume in one dimension. Simulations using a new clutter model/simulator, Ricean clutter model (RiM), better predicted the observed experimental clutter echo statistics when compared with data from a weather simulation model. CPA statistics from the RiM time series simulator matched the CPA statistics from experimental observed data well.

Movement of clutter targets (e.g., swaying trees) was incorporated into a modulated Ricean clutter model

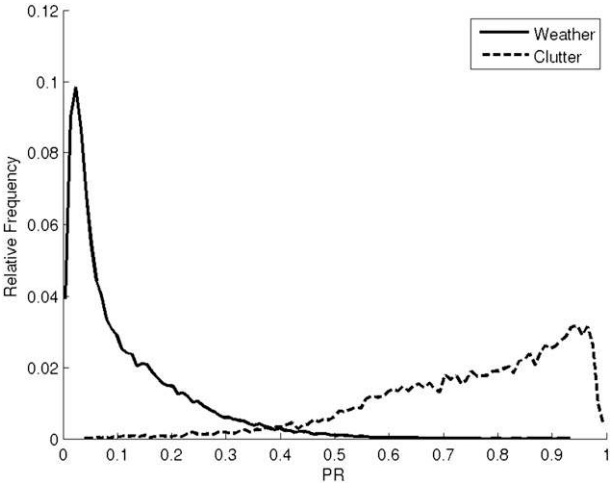

FIG. 18. Relative frequency histograms of KFTG experimental data for $PR^{0.5}$ for the data in Fig. 17.

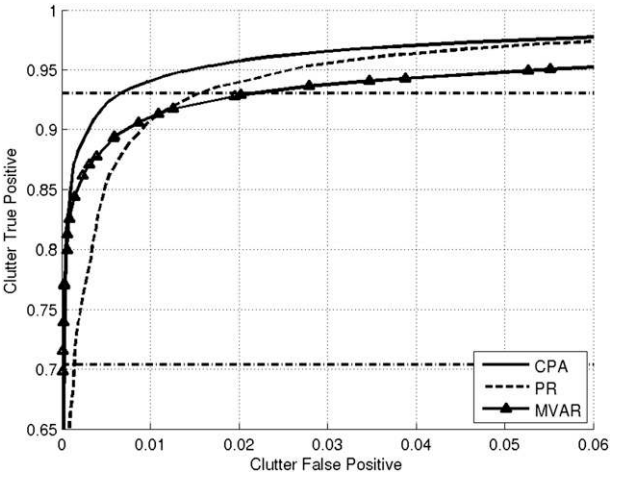

FIG. 20. ROC curves for the data of Figs. 17–19.

(MRM) by allowing the magnitude and phase of the scattering centers to vary. The resulting CPA values remained high enough so that CPA continued to be an effective discriminator of clutter and weather. This indicates why we have found CPA to be a particularly effective and robust ground-clutter identification parameter.

The general observations of this paper are

1) CPA is a function of both mean velocity and spectrum width but is a more robust clutter identification parameter.
2) Since CPA is a vector sum of the time series, it can be calculated directly from non equispaced time series samples.
3) The Gaussian-statistics weather model does not predict the statistics of observed clutter as well as the Ricean-based clutter model (termed the RiM).
4) The observed clutter echoes are not modeled well by summing over an ensemble of Rayleigh-distributed (in amplitude) scattering centers (i.e., the RaM).
5) The KFTG and S-Pol experimentally observed clutter echoes are modeled well using the Ricean model, which indicates that ground-clutter echo is usually characterized by a dominant scatterer. Ground-clutter characteristics from other geographical areas could differ.
6) The MRM simulations indicate that ground-clutter targets can move considerably (with a velocity standard deviation of about 12 m s^{-1} on a sample-to-sample measurement basis) and CPA remains high. Thus, CPA continues to be an effective discriminator of ground clutter versus precipitation.

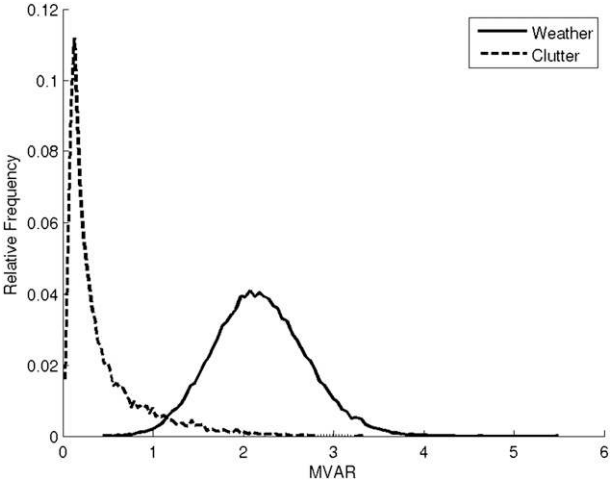

FIG. 19. Relative frequency histograms of KFTG experimental data for MVAR for the data in Fig. 17.

In Part II the CPA parameter is used as a feature field in a fuzzy logic algorithm, termed CMD, for real-time ground-clutter echo identification.

Acknowledgments. The authors thank Tim Crum, Christina Horvat, John Heimer, and Larry Mooney for their assistance in making the collection of time series data from KFTG possible. The authors acknowledge the NCAR EOL/RSF staff for their assistance with data collection on S-Pol, and the technical discussions with Richard Ice and David Ward of the NEXRAD ROC. Evan Ruzanski helped with the theoretical CPA scatter

plots. This work was supported in part by the NOAA Radar Operations Center of Norman, OK. Any opinions, findings, and conclusions or recommendations expressed in this publication are those of the author(s) and do not necessarily reflect the views of the National Science Foundation.

APPENDIX

A Comparison of CPA and a Spectrum Power Ratio

The inequality we hypothesize is

$$\mathrm{CPA} \geq \sqrt{(\mathrm{PR})}. \tag{A1}$$

First, let x_i be a time series sequence and let X_m be the DFT of x_i. Parseval's relationship for the DFT states

$$\sum_i |x_i|^2 = \frac{1}{N}\sum_m |X_m|^2. \tag{A2}$$

Equation (A1) can be expressed as

$$\frac{\left|\sum_{i=1}^{N} x_i\right|}{\left[\sum_{i=1}^{N} |x_i|\right]} \geq \sqrt{\frac{|X_0|^2}{\sum_m |X_m|^2}}. \tag{A3}$$

The right-hand side is rewritten in terms of x_i as (using Parseval)

$$\frac{\left|\sum_{i=1}^{N} x_i\right|}{\left[\sum_{i=1}^{N} |x_i|\right]} \geq \sqrt{\frac{\left|\sum_{i=1}^{N} x_i\right|^2}{N\sum_{i=1}^{N} |x_i|^2}}. \tag{A4}$$

The numerators are equal and the inequality can be rewritten as

$$\left[\sum_{i=1}^{N} |x_i|\right] \leq \sqrt{N\sum_{i=1}^{N} |x_i|^2}. \tag{A5}$$

Dividing both sides by N gives

$$\frac{\left[\sum_{i=1}^{N} |x_i|\right]}{N} \leq \sqrt{\frac{\sum_{i=1}^{N} |x_i|^2}{N}}. \tag{A6}$$

This simply states that the root-mean-square average is greater than the arithmetic mean, a well-known result. Thus we have proven the inequality of Eq. (8).

REFERENCES

Billingsley, J., 2002: *Low Angle Radar Land Clutter: Measurements and Empirical Models*. William Andrew, Inc., 700 pp.

——, and J. Larrabee, 1991: Multifrequency measurements of radar ground clutter at 42 sites. Tech. Rep. 916, MIT Lincoln Laboratory, 212 pp.

Bogush, A., 1989: *Radar and the Atmosphere*. Artech House, 452 pp.

Boothe, R. R., 1969: The Weibull distribution applied to the ground clutter backscatter coefficient, Redstone Arsenal, AL. U.S. Army Missile Command Tech. Rep. RE-69-15, 29 pp.

Bringi, V., and V. Chandrasekar, 2001: *Polarimetric Doppler Weather Radar*. Cambridge University Press, 636 pp.

Chandrasekar, V., V. Bringi, and P. Brockwell, 1986: Statistical properties of dual-polarized signals. Preprints, *23rd Conf. on Radar Meteorology,* Snowmass, CO, Amer. Meteor. Soc., 193–196.

Doviak, R., and D. Zrnić, 1993: *Doppler Radar and Weather Observations*. 2nd ed. Academic Press, 592 pp.

Fang, M., R. Doviak, and V. Melnikov, 2004: Spectrum width measured by WSR-88D: Error sources and statistics of various weather phenomena. *J. Atmos. Oceanic Technol.,* **21,** 888–904.

Frehlich, R., and M. J. Yadlowsky, 1994: Performance of mean-frequency estimators for Doppler radar and lidar. *J. Atmos. Oceanic Technol.,* **11,** 1217–1230.

Geotis, S., and W. Silver, 1976: An evaluation of techniques for automatic ground echo rejection. Preprints, *17th Conf. on Radar Meteorology,* Seattle, WA, Amer. Meteor. Soc., 448–452.

Green, D., and J. Swets, 1966: *Signal Detection Theory and Psychoanalysis*. John Wiley and Sons, 455 pp.

Hubbert, J. C., M. Dixon, and S. Ellis, 2009: Weather radar ground clutter. Part II: Real-time identification and filtering. *J. Atmos. Oceanic Technol.,* **26,** 1181–1197.

Jakeman, E., and P. Pusey, 1976: A model for non-Rayleigh sea clutter. *IEEE Trans. Antennas Propag.,* **24,** 806–814.

Jao, J., 1984: Amplitude distribution of composite terrain radar and the k-distribution. *IEEE Trans. Antennas Propag.,* **32,** 1049–1062.

Keenan, T., J. Wilson, J. Lutz, and P. May, 2006: The restoration of CP-2 in Brisbane, Australia. *Proc. Fourth European Conf. on Radar in Meteorology and Hydrology,* Barcelona, Spain, ERAD, 367–370.

Kerr, D. E., 1951: *Propagation of Short Radio Waves*. Vol. 13, McGraw Hill, 728 pp.

Long, M. W., 2001: *Radar Reflectivity of Land and Sea*. Artech House, 534 pp.

May, P., and R. Strauch, 1998: Reducing the effect of ground clutter on wind profiler velocity measurements. *J. Atmos. Oceanic Technol.,* **15,** 579–586.

Meymaris, G., and J. K. Williams, 2007: Spectrum width estimators for the NEXRAD ORDA: Evaluation and recommendation. Preprints, *23rd Int. Conf. on IIPS,* San Antonio, TX, Amer. Meteor. Soc., 5B.5. [Available online at http://ams.confex.com/ams/pdfpapers/119628.pdf.]

Nguyen, C., D. Moisseev, and V. Chandrasekar, 2008: A parametric time domain method for spectral moment estimation and clutter mitigation for weather radars. *J. Atmos. Oceanic Technol.,* **25,** 83–92.

Norton, K., L. Vogler, W. Mansfield, and P. Short, 1955: The probability distribution of the amplitude of a constant vector plus a Rayleigh-distributed vector. *Proc. IRE,* **43,** 1354–1361.

Passarelli, R. J., and A. Siggia, 1983: The autocorrelation function and Doppler moments: Geometric and asymptotic interpretations. *J. Climate Appl. Meteor.,* **22,** 1776–1787.

Ruck, G., D. Barric, W. Stuart, and C. Krichbaum, 1970: *Radar Cross Section Handbook*. Vol. 2, Plenum Press, 476 pp.

Schaffner, M., P. L. Smith, K. R. Hardy, and K. M. Glover, 1975: Comments on ''Applications of radar to meteorological operations and research.'' *Proc. IEEE,* **63,** 731–733.

Sekine, S., and Y. Mao, 1990: *Weibull Radar Clutter*. Peter Peregrinus Ltd., 190 pp.

Simkins, W., 1984: The ARSR-4 clutter model. Tech. Rep. FAA-E-2763 Appendix A, Federal Aviation Administration.

Steiner, M., and J. Smith, 2002: Use of three-dimensional reflectivity structure for automated detection and removal of nonprecipitating echoes in radar data. *J. Atmos. Oceanic Technol.,* **19,** 673–686.